BIOLOGY OF REPRODUCTION (2015) **93**(5):121, 1–12
Published online before print 2 September 2015.
DOI 10.1095/biolreprod.115.131516

The Histone Methyltransferase Gene *Absent, Small, or Homeotic Discs-1 Like* Is Required for Normal Hox Gene Expression and Fertility in Mice[1]

Michelle L. Brinkmeier,[3] Krista A. Geister,[4] Morgan Jones,[4] Meriam Waqas,[3] Ivan Maillard,[5,6,7] and Sally A. Camper[2,3,5]

[3]*Department of Human Genetics, University of Michigan, Ann Arbor, Michigan*
[4]*Graduate Program in Cellular and Molecular Biology, University of Michigan, Ann Arbor, Michigan*
[5]*Department of Internal Medicine, University of Michigan, Ann Arbor, Michigan*
[6]*Department of Cell and Developmental Biology, University of Michigan, Ann Arbor, Michigan*
[7]*Life Sciences Institute, University of Michigan, Ann Arbor, Michigan*

ABSTRACT

Chromatin remodeling influences gene expression in developing and adult organisms. Active and repressive marks of histone methylation dictate the embryonic expression boundaries of developmentally regulated genes, including the *Hox* gene cluster. *Drosophila ash1* (*absent, small or homeotic discs 1*) gene encodes a histone methyltransferase essential for regulation of *Hox* gene expression that interacts genetically with other members of the trithorax group (TrxG). While mammalian members of the mixed lineage leukemia (*Mll*) family of TrxG genes have roles in regulation of *Hox* gene expression, little is known about the expression and function of the mammalian ortholog of the *Drosophila ash1* gene, *Ash1-like (Ash1l)*. Here we report the expression of mouse *Ash1l* gene in specific structures within various organs and provide evidence that reduced *Ash1l* expression has tissue-specific effects on mammalian development and adult homeostasis. Mutants exhibit partially penetrant postnatal lethality and failure to thrive. Surviving mutants have growth insufficiency, skeletal transformations, and infertility associated with developmental defects in both male and female reproductive organs. Specifically, expression of *Hoxa11* and *Hoxd10* are altered in the epididymis of *Ash1l* mutant males and *Hoxa10* is reduced in the uterus of *Ash1l* mutant females. In summary, we show that the histone methyltransferase *Ash1l* is important for the development and function of several tissues and for proper expression of homeotic genes in mammals.

abdominal fat, axial skeleton, epigenetic, Hoxa11, Hoxd10, *infertility, reproduction*

INTRODUCTION

The regulation of gene activation and inactivation through chromatin remodeling is an evolutionarily conserved phenomenon that is critical for normal development and disease prevention (reviewed in [1, 2]). One means of regulating chromatin access is through the methylation and demethylation of specific lysine residues on histone 3. The methylation of lysine residues H3K4 and H3K36 is associated with gene activation, while methylation of H3K27 corresponds to gene repression. Gene fusions in histone methyltransferase genes cause human disease, including members of the mixed lineage leukemia family (MLL) (reviewed in [3]). Analysis of mouse models of loss-of-function for these genes has provided valuable insights into their mechanism of action and pathophysiology of disease [4–6].

The *Drosophila ash1* gene (absent, small, or homeotic 1) encodes a member of the trithorax group (TrxG) of proteins that maintain transcription by histone modification and chromatin remodeling. MLL1 is the founding member of the TrxG family in mammals, and *Ash1l* (absent, small, or homeotic 1-like) is the mouse ortholog of the *Drosophila ash1* gene. Both *Drosophila* ASH1 and mammalian ASH1L proteins contain several highly conserved functional domains, including AT hook domains, which modulate chromatin structure and DNA binding; the Pre-SET (Su [var] 3–9, Enhancer of zeste, and trithorax), SET, and Post-SET domains, which are involved in histone methyltransferase activity; the bromodomain, important for protein-histone association; and the PHD domain, a zinc finger domain that could be important for protein-protein or DNA-protein interactions. ASH1 methylates H3K4 and H3K36, activating gene expression by counteracting the repressive state established by the polycomb group (*PcG*) proteins [7–13]. There is conflicting data about the methyltransferase specificity of ASH1L, and most of the information comes from in vitro studies. It has been identified at active *Hox* genes in HeLa cells and embryonic stem cells [14, 15]. Thus, aspects of ASH1 and ASH1L biochemical activity and function in gene regulation are conserved.

The gene *ash1* was identified in *Drosophila* mutants with late larval stage lethality and homeotic transformations of structures derived from imaginal discs [16, 17]. Each mutant allele causes various homeotic transformations, including the third thoracic segment to the second thoracic segment, antenna to leg, or genitalia to leg [16, 17]. Inducible alleles permit ascertainment of *ash1* function in adult *Drosophila*. Using this approach, *ash1* was shown to be critical for normal oogenesis, egg laying, and female fertility [16]. Thus, *ash1* mutations have highly pleiotropic effects in *Drosophila* organ development and adult functions.

Only one mutant allele of *Ash1l* has been reported in mammals. Mutants lacking the SET domain exhibit homeotic transformations of the axial skeleton and exhibit a posterior shift in expression of selected *Hox* genes: *b4*, *d4*, and *a4* [15]. Effects on other organs were not reported. This mutant only

[1]This work was supported by NIH grant number R37-HD30428-19 (to S.A.C.) and fellowships from the University of Michigan Regents and the Reproductive Science Program (to K.A.G.).
[2]Correspondence: Sally A. Camper, 4909 Buhl Bldg., 1241 Catherine St., Dept. Human Genetics, University of Michigan Medical School, Ann Arbor, MI 48109-5618. E-mail: scamper@umich.edu

Received: 13 May 2015.
First decision: 29 June 2015.
Accepted: 1 September 2015.

eISSN: 1529-7268 http://www.biolreprod.org
ISSN: 0006-3363

reveals SET domain-dependent functions, and SET domain-independent functions exist in several MLL family members [18]. Both *ash1* and *Ash1l* are expressed in a variety of developmental stages and adult organs [13, 15, 16, 19, 20], although no systematic studies have been done in mammals. Here, we report on *Ash1l* gene expression in mice, a novel *Ash1l* loss of function allele, and the effects of *Ash1l* deficiency on male and female reproductive organ development and function.

MATERIALS AND METHODS

Generation of Mice and Genotyping

The gene trap ES cell line AL0395 was obtained from The Wellcome Trust Sanger Institute. This gene trap has an insertion of the pGT01xf vector in intron 1 of the *Ash1l* locus [21]. The ES cell line was injected into donor blastocysts from matings of C57BL/6J × (C57BL/6J x DBA/2J) F1 mice (Jackson Laboratory) by The University of Michigan Transgenic Animal Model Core. Chimeric males with the highest percentage of agouti fur were bred to C57BL/6J females to establish the gene trap mouse line. The mice were housed in specific pathogen-free conditions in ventilated cages with automatic watering and fed Purina 5020 chow ad libitum. All the procedures were in accordance with The University of Michigan University Committee on the Use and Care of Animals guidelines.

An extensive set of PCR forward primers designed against nonrepetitive areas of the *Ash1l* intron 1 were tested individually with a reverse primer within the gene trap vector. Amplification products unique to the gene trap allele were sequenced and compared to the mouse reference genome (Ensembl release 49). The insertion site of the gene trap is 14 653 bp into intron 1. This information was used to establish a PCR assay for genotyping that specifically amplifies the wild-type and gene trap alleles. The wild-type allele was amplified with primers within intron 1 that span the gene trap insertion site: forward 5′-GTCTTGATAAATAAATGGCGATAA-3′ and reverse 5′-AGGTGCTGG GAAACAAACTAAT-3′. A forward primer, 5′-GTCTTGATAAA TAAATGGCGATAA-3′, within intron 1 and a reverse primer, 5′-AGTATCGGCCTCAGGAAGATCG-3′, within the gene trap vector were used to amplify the gene trap allele. A multiplex PCR was used to amplify both alleles under the following conditions: 94°C for 2 min followed by 30 cycles of 94°C for 45 sec, 52°C for 45 sec, and 72°C for 1 min, followed by a final extension of 72°C for 10 min. PCR products were visualized on a 1% agarose gel. The wild-type primer set amplified a 645 bp fragment, and the gene trap primer set amplified a 1.3 kb fragment.

Female Fertility Studies

Female fertility was assayed by housing two $Ash1l^{GT/GT}$ females and one $Ash1l^{+/+}$ male per cage for 3 mo. The number of litters produced per female was compared to heterozygote breeding cages over the same 3-mo period. Fertilization rates were determined by superovulating 3-wk-old $Ash1l^{+/+}$ and $Ash1l^{GT/GT}$ females and housing them overnight with C57BL/6J males and checking for plugs the following morning [22]. The number of fertilized eggs was compared to the total number of eggs collected, as previously described [23]. To assess the uterine environment, fertilized eggs were cultured to blastocysts and transferred to the uteri of pseudopregnant females. The number of pups born from fertilized eggs from superovulated $Ash1l^{GT/GT}$ females was compared to those born from $Ash1l^{+/+}$ females.

Chicago Sky Blue Tail Injection

The ability of the uterine environment to form decidua was tested by mating 6- to 8-wk-old $Ash1l^{+/+}$ and $Ash1l^{GT/GT}$ female mice to C57BL/6J male mice. On 5.5 Days Postcoitum (dpc), the tail vein of female mice was injected with 100 μl of 0.9% Chicago Sky Blue 6B diluted in 1× phosphate buffered saline (PBS). Mice were euthanized after 10 min, and the presence or absence of decidua was visualized by the accumulation of dye at the implantation sites.

Vaginal Smears

Vaginal smears were performed on 8-wk-old females at the same time, in the morning, each day for a week. Vaginal openings were flushed with 1× PBS. The fluid was spread onto microscope slides, air dried, and fixed for 20 sec with 100% methanol. The stages of the estrous cycle were visualized using the Leica Leitz DMRB compound microscope.

Tissue Preparation

Tissues from neonates and adults were dissected and fixed in 1× PBS and 4% formaldehyde. Ovaries, uteri, epididymis, vas deferens, and eyelids were fixed for 2 h. Testes fixation was carried out overnight at 4°C after making a thin slice in the outer capsule layer to facilitate penetration of the fixative. Skin was removed from the heads of neonates to facilitate penetration of the fixative overnight at 4°C. All the tissues for paraffin embedding were then rinsed twice in 1× PBS, dehydrated in stages to 70% ethanol, and processed in the Miles Scientific VIP 2000 Tissue Processor and a Shandon Histocentre 2 paraffin embedding station (Thermo Electron Co.). Tissues were sectioned to 6 μm thickness using the American Optical 820 Spencer microtome, mounted onto Super Frost Plus microscope slides (Fisher Scientific), and either stained with hematoxylin and eosin or processed for immunohistochemistry or in situ hybridization, as described below. The number of uterine glands per unit area was determined using Image J Quant software.

Immunohistochemistry

Immunohistochemistry was performed on paraffin sections using the following antibodies: rabbit-anti-ASH1L (uterus, ab4477; AbCam), rabbit-anti-ASH1L 296 (epididymis, a gift from Dr. Greg Gregory and Dr. Gerd Blobel [14]), rabbit anti-FOXA2 (ab40874; Abcam), rabbit anti-cleaved CASPASE 3 (9661S; Cell Signaling Technology), mouse anti-CYCLIND1 (sc-8396; Santa Cruz), and rabbit anti-CYCLIND2 (sc-593; Santa Cruz). All the antibodies were used at a 1:100 dilution and processed using the TSA-FITC Immunostaining kit (Perkin Elmer Cetus) as previous described [24]. Antibody expression was visualized using a Leica Leitz DMRB compound microscope with Image Q or Leica Application Suite, LAS v2.7.

In Situ Hybridization

In situ hybridization was performed on paraffin sections using a digoxygenin-UTP (Life Technologies) labeled probe that recognizes from 300 to 1370 bp of the *Hoxa10* transcript. Briefly, *Hoxa10* forward (5′-ATTTTTCCTGATGAAACTTCC-3′) and reverse (5′-GGAAATCCAAACAA TATCTCC-3′) PCR primers were used to amplify *Hoxa10* transcript from adult uterus cDNA and cloned using the pGEM T Easy Cloning System (Promega). The identity of the cloned transcript was confirmed, from both SP6 and T7 ends, using Sanger sequencing. The *Hoxa10* cDNA plasmid was restriction enzyme digested with *Spe*I and labeled with T7 polymerase (Promega) to generate the antisense transcript and digested with *Sac*II and labeled with SP6 (Promega) to generate the sense transcript. *Hoxa10* antisense- and sense-labeled probes were diluted 1:100 in hybridization solution and processed as previously described [25].

Male Fertility Studies

We assessed male fertility by natural mating and in vitro fertilization. Either an $Ash1l^{GT/GT}$ or $Ash1l^{+/+}$ male was housed with two $Ash1l^{+/+}$ females for 3 mo. The number of litters produced per cage during the allotted time was compared. The in vitro fertilization rate was determined by incubating sperm collected from $Ash1l^{+/+}$ or $Ash1l^{GT/GT}$ males with eggs from superovulated 3-wk-old $Ash1l^{+/+}$ females. The number of fertilized eggs that survived to the blastocyst stage was compared to the total number of eggs used. In vitro fertilization was performed using the standard JAX laboratory protocol [26–28].

Real-Time PCR

Epididymis, vas deferens, uteri, and embryos collected at 14.5 dpc were dissected and stored in RNA Later (Ambion, Life Technologies) at −20°C. The epididymis was dissected under a Leica MZ75 dissecting microscope and segmented into the initial segment, corpus, caput, cauda, and vas deferens based on published boundaries [29]. The observation of a vaginal plug in the morning was considered to be 0.5 dpc. Embryos were dissected as previously described [22]. RNA was isolated and DNase I treated using the protocols provided in the RNA 4 PCR kit (Applied Biosystems, Life Technologies). The cDNA was generated using the Superscript II system from Invitrogen (Life Technologies). Specifically, RNA and oligo dT primers were denatured at 70°C for 10 min and then placed on ice; 100 mM dithiothreitol, 10 mM dNTPs, 5× first-strand buffer, and 1 unit Superscript II were added to the RNA primer mix. Samples were incubated at 42°C for 50 min and then heat inactivated for 10 min at 70°C. Samples without Superscript II were included as negative controls. The quality of the cDNA reaction and effectiveness of the DNase I treatment of the RNA was tested using PCR with primers to the housekeeping gene *Hprt*.

Real-time PCR was carried out using Taqman Gene Expression Assays for *Ash1l* (Mm01212715_m1), *Hoxa9* (Mm00439364_m1), *Hoxa10* (Mm00433966_m1), *Hoxa11* (Mm00439370_m1), *Hoxc9* (Mm00433972_m1), *Hoxd13* (Mm00433973_m1), *Hoxd10* (Mm00442839_m1), *Hoxc4* (Mm00442838_m1), and *Gapdh* (4308316) from Applied Biosystems. The real-time PCR reaction was set up with triplicate cDNA samples and Taqman dNTP Master Mix (Applied Biosystems). Amplification of experimental primer sets in individual cDNA samples was normalized to the amplification of *Gapdh* in that sample. Triplicates containing the Master Mix and cDNA without the Taqman primer sets were used as a negative control. Fold change of $Ash1l^{GT/GT}$ compared to $Ash1l^{+/+}$ mice was calculated as described previously [30].

X-Gal Staining

Epididymis and vas deferens tissues were dissected from $Ash1l^{+/+}$ and $Ash1l^{GT/GT}$ males and fixed for 1 h in buffered 4% formaldehyde. After washing in 1× PBS, tissue samples were incubated briefly in a LacZ wash buffer consisting of 2 mM $MgCl_2$ and 2% NP-40 in 0.1 M sodium phosphate buffer (pH 7.3). Endogenous and gene trap LacZ expression was visualized by staining overnight, in the dark, in 1 mg/ml X-gal (Invitrogen) diluted in dimethylformamide with LacZ wash buffer containing 0.2% potassium ferrocyanide and 0.16% potassium ferricyanide. After staining, tissue samples were rinsed in Lac Z wash buffer and postfixed overnight at 4°C in buffered 4% formaldehyde and processed for paraffin sections as previously described.

Whole Mount In Situ Hybridization

Epididymides from 3-wk-old mutant and wild-type males were dissected and fixed in buffered 4% formaldehyde for 2 h. After fixation, samples were rinsed in 1× PBS, dehydrated through an increasing series of methanol, and stored at −20°C. At the start of the experiment, the samples were rehydrated in 75%, 50%, and 25% methanol in 1× PBS with 0.5% Triton X100 (PBST). Samples were rinsed in PBST then digested in 4.5 μg/ml proteinase K for 13 min at room temperature. Digestion was halted with 2 mg/ml glycine in PBST. Samples were postfixed in buffered 4% formaldehyde and 0.2% glutaraldehyde. After fixation, samples were incubated for 3 h in hybridization solution containing 50% formamide, 1.3× SSC buffer, 5 mM ethylenediaminetetraacetic acid, 50 μg/ml yeast tRNA, 0.5% 3-[(3-cholamidopropyl)dimethylammonio]-1-propanesulfonate, and 100 μg/ml heparin at 65°C. Samples were then incubated in a 1:100 dilution of digoxygenin-labeled *Ash1l* and *Hoxa11* riboprobes overnight at 70°C. The next day, samples went through a series of washes in 2× SSC followed by maleic acid buffer. Samples were blocked in 10% normal goat serum/1% Roche Blocking Powder in PBST for 3 h at 4°C. The antibody block was replaced with a 1:5000 dilution of anti-digoxygenin-alkaline phosphatase antibody and incubated overnight at 4°C. The next day, samples were washed in 0.1% bovine serum albumin in PBST then prepared for developing through a series of washes in a buffer containing 100 mM Tris, pH 9.5, 100 mM NaCl, and 50 mM $MgCl_2$. Samples were developed for 11 h in a 1:50 dilution of nitro blue tetrazolium/5-bromo-4-chloro-3-indolyl phosphate staining solution in the same buffer. Background staining was removed through a series of dehydration then rehydration steps in methanol and PBST.

Statistical Analysis

The *P*-value for analysis of perinatal lethality in each age group was calculated using the chi square test, comparing each group to the expected Mendelian ratios. The *P*-values for body weight, percent abdominal fat, number of motile sperm, and fertilization rates were formulated using the sum of ranks Mann-Whitney test. The *P*-values for the real-time PCR were determined using the Student *t*-test. For all data, * represents $P < 0.01$, ** represents $P < 0.001$, and *** represents $P < 0.0001$.

RESULTS

Ash1l$^{GT/GT}$ Mutants Have Reduced Viability and Other Abnormalities

The ES cell line AL0395 contains a gene trap cassette in intron 1 of the mouse *Ash1l* gene, and it was used to generate mice deficient in *Ash1l*. Transcripts that splice into the gene trap lack the coding regions for all of the known functional domains of the ASH1L protein. These include the AT hook domains, the SET-associated domains that confer histone methyltransferase activity, the bromodomain, and the PHD domain (Fig. 1A). $Ash1l^{+/GT}$ males and females were bred, and over 1000 pups were genotyped to determine the viability of the mutants. The expected Mendelian distribution of genotypes (1:2:1) was observed during embryonic development through Postnatal Day 7 (P7). $Ash1l^{GT/GT}$ mutants were significantly underrepresented after P7 and older. At P21, 25% of the pups are expected to be $Ash1l^{GT/GT}$ but only 14% were observed (Fig. 1B).

Surviving $Ash1l^{GT/GT}$ mutants were significantly smaller than wild-type mice at P14, and at weaning, they were only 60% the weight of $Ash1l^{+/+}$ littermates (Fig. 1, C and D). The lower weight of surviving $Ash1l^{GT/GT}$ mutants was primarily due to reduced growth, although fat deposition is also altered. Abdominal fat from 2- to 3-mo-old $Ash1l^{+/+}$ and $Ash1l^{GT/GT}$ males was dissected, weighed, and compared to the overall body weight. The percentage abdominal fat in $Ash1l^{GT/GT}$ males was consistently less than 1% while the percentage abdominal fat in wild-type littermates ranged from 1.5% to 4.2% (Fig. 1E). In addition, $Ash1l^{GT/GT}$ adult mice exhibited a hematopoietic stem cell defect, although it did not progress to spontaneous bone marrow failure [31]. Thus, the reduced viability and growth are apparently associated with an overall failure to thrive.

Ash1l deficiency affects eyelid and skeletal development. Mice are born with their eyelids closed, and eyelid development is completed postnatally [32]. ASH1L immunoreactivity was strong in the meibomian glands of normal eyelids, which are necessary for eye lubrication. Adult *Ash1l* mutants lacked these glands and developed chronic inflammation or blepharitis, similar to that described for Kruppel-like factor 5 (*Klf5*) deletion in the ocular surface ectoderm (Supplemental Fig. S1; Supplemental Data are available online at www.biolreprod.org) [33]. Vertebral abnormalities were detected in the thoracic region, specifically an additional rib was frequently attached to the ribcage and the ribs were attached in a staggered manner to the sternum (Supplemental Fig. S2). These skeletal abnormalities are different from those observed in the *Ash1l* SET domain mutants [15].

Ash1l$^{GT/GT}$ Females Are Infertile due to Defects in Uterine Development

No $Ash1l^{GT/GT}$ females (n = 7) gave birth to pups after being housed with normal males for 3 mo, indicating that they were infertile (Table 1). We analyzed the effect of *Ash1l* deficiency on hypothalamic-pituitary-gonadal axis function by examining the ovaries and the estrous cycle. Ovaries were evaluated for the presence of ovarian follicles and corpora lutea by hematoxylin and eosin staining. All the stages of folliculogenesis were observed in $Ash1l^{GT/GT}$ females, and the ovaries also produced corpora lutea, consistent with ovulation (Fig. 2A). In addition, cellular features diagnostic of all stages of the estrous cycle were visualized in vaginal smears (data not shown), which is consistent with normal neuroendocrine axis function. Taken together, these observations suggest that the defect was not in the hypothalamic-pituitary-gonadal axis.

To test the viability of the mutant eggs, $Ash1l^{+/+}$ and $Ash1l^{GT/GT}$ 4-wk-old females were superovulated and then housed overnight with C57BL6/J males. Eggs were collected and cultured to the blastocyst stage. No difference in the fertilization rate was observed, indicating that *Ash1l* mutant eggs are normal (Table 1). Embryo transfers were conducted to compare the function of eggs and uteri from normal and mutant animals. $Ash1l^{+/+}$ and $Ash1l^{GT/GT}$ females were superovulated, bred to C57BL6/J males, and blastocysts were collected and transferred into normal pseudopregnant females. Fertilized

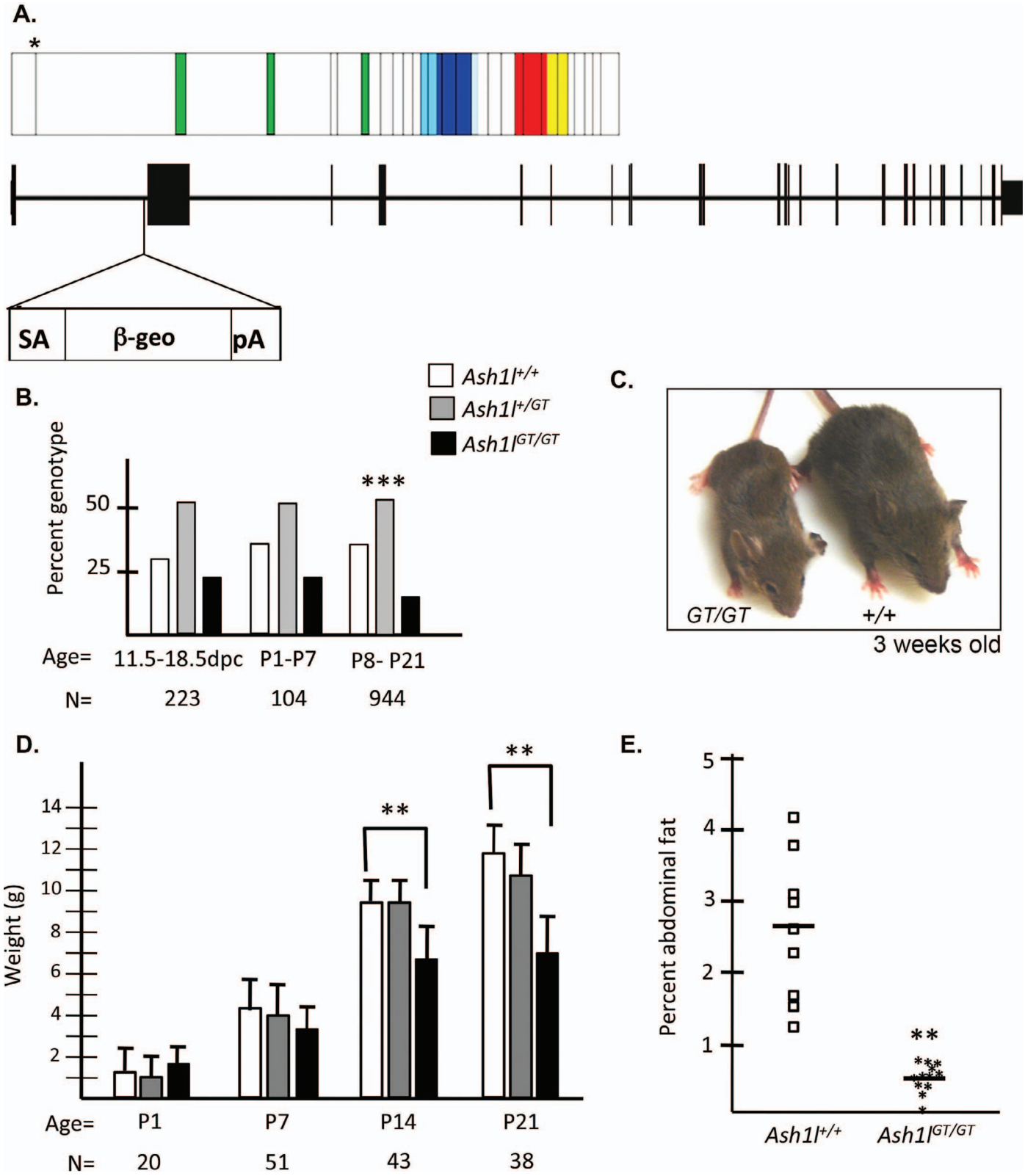

FIG. 1. *Ash1l*$^{GT/GT}$ mutants have increased postnatal lethality and reduced body weight. **A**) ASH1L protein (top) and gene (bottom) structures. In the protein structure diagram, the portion of the protein encoded by each exon is separated by a thin black line. The gene trap vector was inserted into intron 1 of the *Ash1l* locus. Splicing into the gene trap would result in a truncated protein (star denotes end of gene trap protein) void of the AT hooks (green), Pre-SET, SET, and Post-SET domains (blues), the Bromo domain (red), and the PHD domain (yellow). **B**) The genotype distributions at 11.5–18.5 dpc, P1–P7, and P8–P21 are displayed for *Ash1l*$^{+/+}$ (white), *Ash1l*$^{+/GT}$ (gray), and *Ash1l*$^{GT/GT}$ (black) mice. The number of mice in each group is indicated (n). **C**) Size comparison of 3-wk-old *Ash1l*$^{GT/GT}$ (left) and littermate *Ash1l*$^{+/+}$ control (right). **D**) Body weights at P1, P7, P14, and P21 were compared for each genotype. The number of mice in each group is indicated (n). **E**) Percent abdominal fat was calculated by dividing the weight of the abdominal fat by the overall body weight. The percent abdominal fat from each individual *Ash1l*$^{+/+}$ male (n = 9) and each individual *Ash1l*$^{GT/GT}$ male (n = 11) are indicated with open boxes and stars, respectively. The bar represents the median of the group.

TABLE 1. *Ash1l*$^{GT/GT}$ females are infertile but mutant eggs can be fertilized.

Fertility study	+/+[a]	+/GT[a]	GT/GT	Result
Presence of stages of estrous cycle (no. females)[b]	Yes (2)	ND	Yes (3)	Normal
Litters produced per no. females[c]	ND	21/8 = 2.6	0/7 = 0	Infertile
Fertilization rate (no. females)[d]	35% (3)	ND	28% (3)	Normal
Pups born in a wild-type uterine environment (no. females)[e]	31 (2)	ND	19 (4)	Normal

[a] ND, not determined.
[b] Stages of estrous cycle determined by vaginal smears.
[c] Litters produced from two mutant females housed with one wild-type male for 3 mo (= litters/female).
[d] Eggs were collected from superovulated females bred to wild-type males. The number of fertilized eggs was compared to the total number collected.
[e] Number of pups born from fertilized eggs collected from either +/+ or GT/GT superovulated females/total pups and transplanted into pseudopregnant wild-type females.

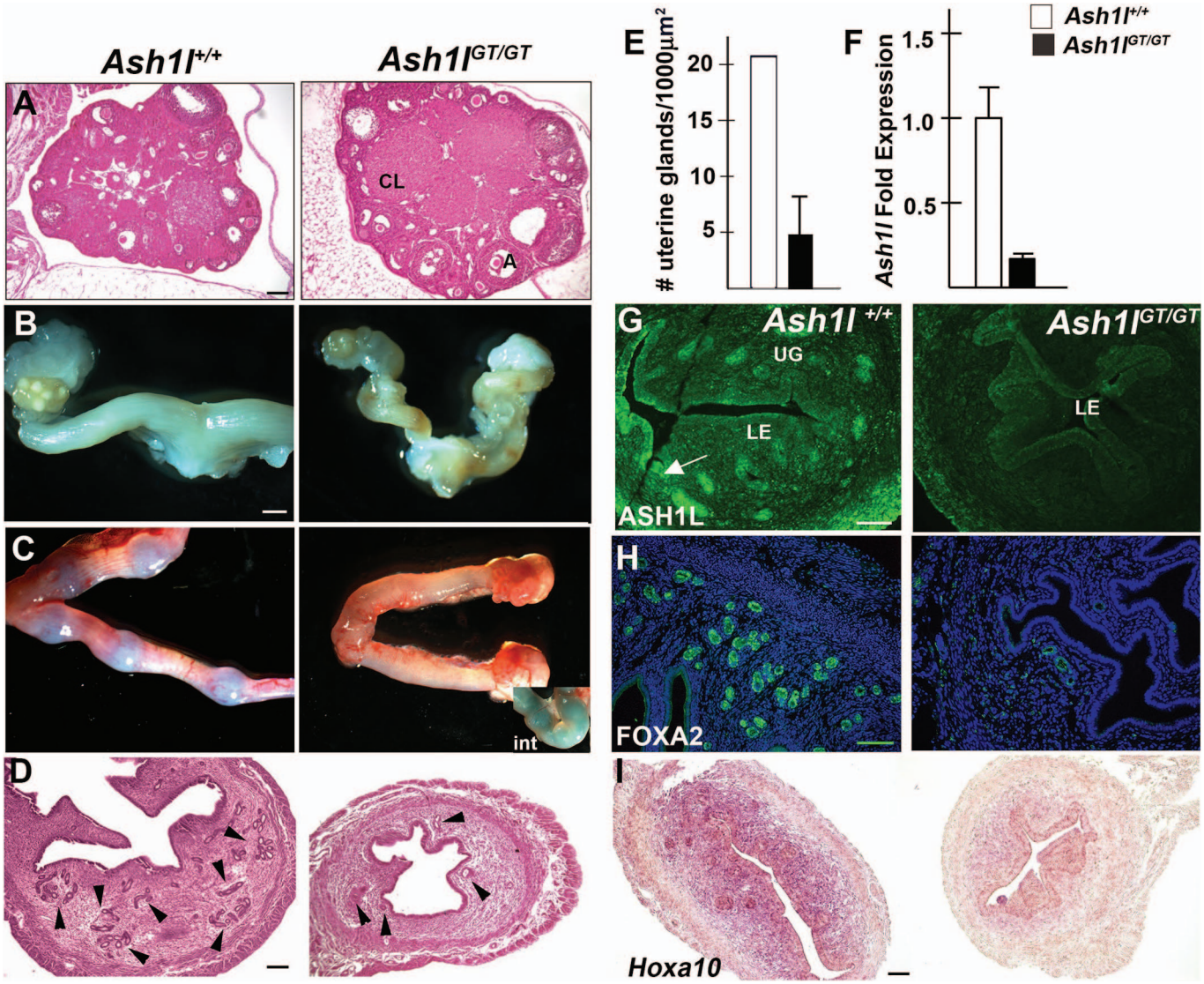

FIG. 2. *Ash1l*$^{GT/GT}$ female display uterine insufficiency. **A**) Hematoxylin and eosin staining of ovary sections from 6-wk-old *Ash1l*$^{+/+}$ (left) and *Ash1l*$^{GT/GT}$ (right) mice. CL, corpus luteum; A, antral follicle. Bar = 100 μm. **B**) Uterine horns from 4-mo-old *Ash1l*$^{+/+}$ (left) and *Ash1l*$^{GT/GT}$ (right) mice. Bar = 1 mm. **C**) Decidualization sites visualized by Chicago Sky Blue dye in *Ash1l*$^{+/+}$ uterus at 5.5dpc compared to *Ash1l*$^{GT/GT}$ uterus at 5.5dpc. Inset in *Ash1l*$^{GT/GT}$ represents a portion of the intestine as a control for the Chicago Sky Blue 6B injection. **D**) Hematoxylin and eosin staining of uterus sections from 3-mo-old *Ash1l*$^{+/+}$ (left) and *Ash1l*$^{GT/GT}$ (right) mice. Arrowheads indicate location of uterine glands. Bar = 100 μm. **E**) Quantification of uterine glands in 3-mo-old *Ash1l*$^{+/+}$ compared to three *Ash1l*$^{GT/GT}$. **F**) *Ash1l* real-time PCR using 4-wk-old uterus cDNA from four *Ash1l*$^{+/+}$ mice (averaged in white bar) compared to four *Ash1l*$^{GT/GT}$ mice (averaged in black bar). The bars represent fold expression change compared to *Ash1l*$^{+/+}$. **G**) ASH1L antibody staining of 3-wk-old uterus section from *Ash1l*$^{+/+}$ (left) and *Ash1l*$^{GT/GT}$ (right) mice. **H**) FOXA2 immunohistochemistry on 3-mo-old *Ash1l*$^{+/+}$ (left) and *Ash1l*$^{GT/GT}$ (right). LE, luminal epithelium; UG, uterine glands. Magnification bar = 50 μm. **I**) *Hoxa10* in situ hybridization of 3-wk-old uterus section from *Ash1l*$^{+/+}$ (left) and *Ash1l*$^{GT/GT}$ (right) mice. Bar = 100 μm.

eggs from both *Ash1l*$^{+/+}$ and *Ash1l*$^{GT/GT}$ females developed in the wild-type uterine environment and yielded newborn pups, indicating that *Ash1l* mutant eggs are viable (Table 1). Thus, the infertility of *Ash1l*$^{GT/GT}$ females is due to the inability of the mutant uterine environment to support a pregnancy.

To determine the underlying cause of uterine failure in *Ash1l*-deficient mice, we examined the uterus histologically and assessed function in supporting implantation. Uteri from *Ash1l*$^{GT/GT}$ adults were smaller and appeared twisted compared to *Ash1l*$^{+/+}$ controls (Fig. 2B). Sites of decidualization are detected by injecting Chicago Sky Blue 6B injected into the tail vein of female *Ash1l*$^{+/+}$ and *Ash1l*$^{GT/GT}$ mice at 5.5 dpc. Blue dye indicative of implantation and decidualization was obvious in the uteri of *Ash1l*$^{+/+}$ mice but not *Ash1l*$^{GT/GT}$ mice (n = 3) (Fig. 2C). The stromal layer of the uterus was thinner in mutants, and there were substantially fewer endometrial uterine glands within it (Fig. 2D). The difference in the number of uterine glands was quantitated in serial sections spanning an entire uterine horn from *Ash1l*$^{+/+}$ and *Ash1l*$^{GT/GT}$ females and normalized for differences in uterine area (Fig. 2E). There was a 4-fold reduction in uterine glands in mutants. ASH1L is normally expressed in these glands, and there is little *Ash1l* RNA or protein in the mutants (Fig. 2, F and G). This is consistent with an important role for ASH1L in developing uterine glands.

We examined expression of *Foxa2* and *Hoxa10,* two genes that are critical for normal uterine development. We analyzed FOXA2 expression in the uterus of *Ash1l*$^{+/+}$ and *Ash1l*$^{GT/GT}$ females at 3 wk of age (n = 2 *Ash1l*$^{+/+}$, n = 4 *Ash1l*$^{GT/GT}$) and as adults (n = 3 *Ash1l*$^{+/+}$, n = 3 *Ash1l*$^{GT/GT}$). As expected, FOXA2 immunostaining was robust in the uterine glands of normal mice (Fig. 2H) [34]. In the mutants, there was a trace of FOXA2 immunoreactivity in the few existing uterine glands, but it was significantly reduced. *Hoxa10,* a target of *Ash1l* in cell culture, is expressed in the stroma of the uterus and is essential for implantation in the mouse [35, 36]. *Hoxa10* expression was analyzed in *Ash1l*$^{+/+}$ (n = 4) and *Ash1l*$^{GT/GT}$ (n = 4) uteri at 3 wk of age. Abundant *Hoxa10* staining was detected in the stroma of the wild type, but substantially reduced levels were detected in all mutant stroma (Fig. 2I). Therefore, ASH1L is required for proper uterine development, including the uterine glands required for implantation, and for normal *Hoxa10* expression in the stroma.

Ash1l$^{GT/GT}$ *Males Exhibited Reduced Fertility due to Defects in the Epididymis*

Four *Ash1l*$^{+/GT}$ males were housed with two wild-type females each over a 3 mo period. They sired 21 litters, while twice as many *Ash1l*$^{GT/GT}$ males (n = 8) sired a combined total of only three litters over the same time period (Table 2). This represents a 90% reduction in fertility in *Ash1l*$^{GT/GT}$ males. Immunohistochemistry for gonadotropins was indistinguishable in *Ash1l*$^{GT/GT}$ and wild-type littermate pituitaries, indicating no obvious change in gonadotropes (data not shown). There were also no obvious morphological abnormalities in *Ash1l*$^{GT/GT}$ testis (data not shown). Leydig cells appeared normal, and the sperm in the tubules appeared qualitatively similar to the wild type, consistent with normal pituitary stimulation of testosterone production and spermatogenesis.

To determine the cause(s) of male infertility we assessed the ability of sperm collected from the entire epididymis of *Ash1l*$^{+/+}$, *Ash1l*$^{+/GT}$, and *Ash1l*$^{GT/GT}$ males to fertilize normal eggs in vitro. Sperm were incubated with eggs from superovulated wild-type females, and the eggs were cultured to the blastocyst stage. Unfertilized eggs undergo fragmentation and die. While there was a wide range of in vitro fertilization rates for all genotypes (Table 2), there was no difference in the fertilization rates of *Ash1l*$^{+/+}$ and *Ash1l*$^{GT/GT}$ sperm based on the Mann-Whitney sum of ranks statistical analysis (Supplemental Fig. S3). Thus, *Ash1l*-deficient mice produce sperm capable of fertilization.

The epididymis provides a protective and nurturing environment important for sperm maturation prior to storage in the cauda and exit through the vas deferens (reviewed in [37, 38]). The performance of the epididymis can be analyzed indirectly by comparing the quality of the sperm within the epididymis to those exiting through the vas deferens. We evaluated the number of motile sperm in both the epididymis and vas deferens of *Ash1l*$^{+/+}$ and *Ash1l*$^{GT/GT}$ and present the results in a scatter plot (Fig. 3, A and B). Based on the Mann-Whitney sum of ranks statistical analysis, there were no significant changes in motility or number between sperm collected from normal and mutant epididymis ($P = 0.23$), but the number of motile sperm in the vas deferens was significantly reduced in *Ash1l*$^{GT/GT}$ mice ($P = 0.006$).

We examined the epididymis to determine the cause of the sperm maturation defect. Sperm travels through four regions of the epididymis with distinct characteristics before reaching the ductus deferens of the vas deferens. These regions are the initial segment, caput, corpus, and cauda. Each segment of the epididymis contains a unique composition of epididymal fluid that progressively promotes the maturation and sperm motility [39]. The epididymides from four *Ash1l*$^{+/+}$, 11 *Ash1l*$^{+/GT}$, and 20 *Ash1l*$^{GT/GT}$ adult males were dissected, stained with X-gal, taking advantage of the endogenous β-galactosidase enzymatic activity present in wild-type epididymides and from the LacZ cassette in the gene trap alleles of the mutant, and visualized each of the regions of the epididymis and the ductus deferens. The structure of the initial segment, caput, corpus, cauda, and ductus deferens from the *Ash1l*$^{+/+}$ and all of the *Ash1l*$^{+/GT}$ males appeared normal (Fig. 3C and data not shown) [29]. In contrast, 17 out of 20 epididymides from the *Ash1l*$^{GT/GT}$ males exhibited a morphological transformation from corpus to caput, a widening of the cauda, and a twisting of the ductus deferens (Fig. 3C). These transformations appear similar to the posterior transformations that occur in *Hoxa10*$^{-/-}$ and in *Hoxa9,10,11* mutant males in that the corpus resembled the caput, the cauda

TABLE 2. *Ash1l*$^{GT/GT}$ males exhibit reduced fertility.

Fertility study	+/+[a]	+/GT	GT/GT	Result
Litters produced per no. of males[b]	ND	21/4 = 5.25	3/8 = 0.375	Reduced
In vitro fertilization rate (no. males)[c]	15%–94% (7)	18%–73% (3)	0%–62% (8)	Normal
Epididymis: motile sperm count (no. males)	22×10^6 to 119×10^6 (5)	61×10^6 (1)	11×10^6 to 42×10^6 (5)	Normal
Vas deferens: motile sperm count (no. males)	2×10^6 to 9×10^6 (2)	3×10^6 (1)	5×10^5 to 2×10^6 (5)	Reduced

[a] ND, not determined.
[b] Litters produced from two wild-type females for 3 mo per male (= litters/male).
[c] Blastocysts/total eggs.

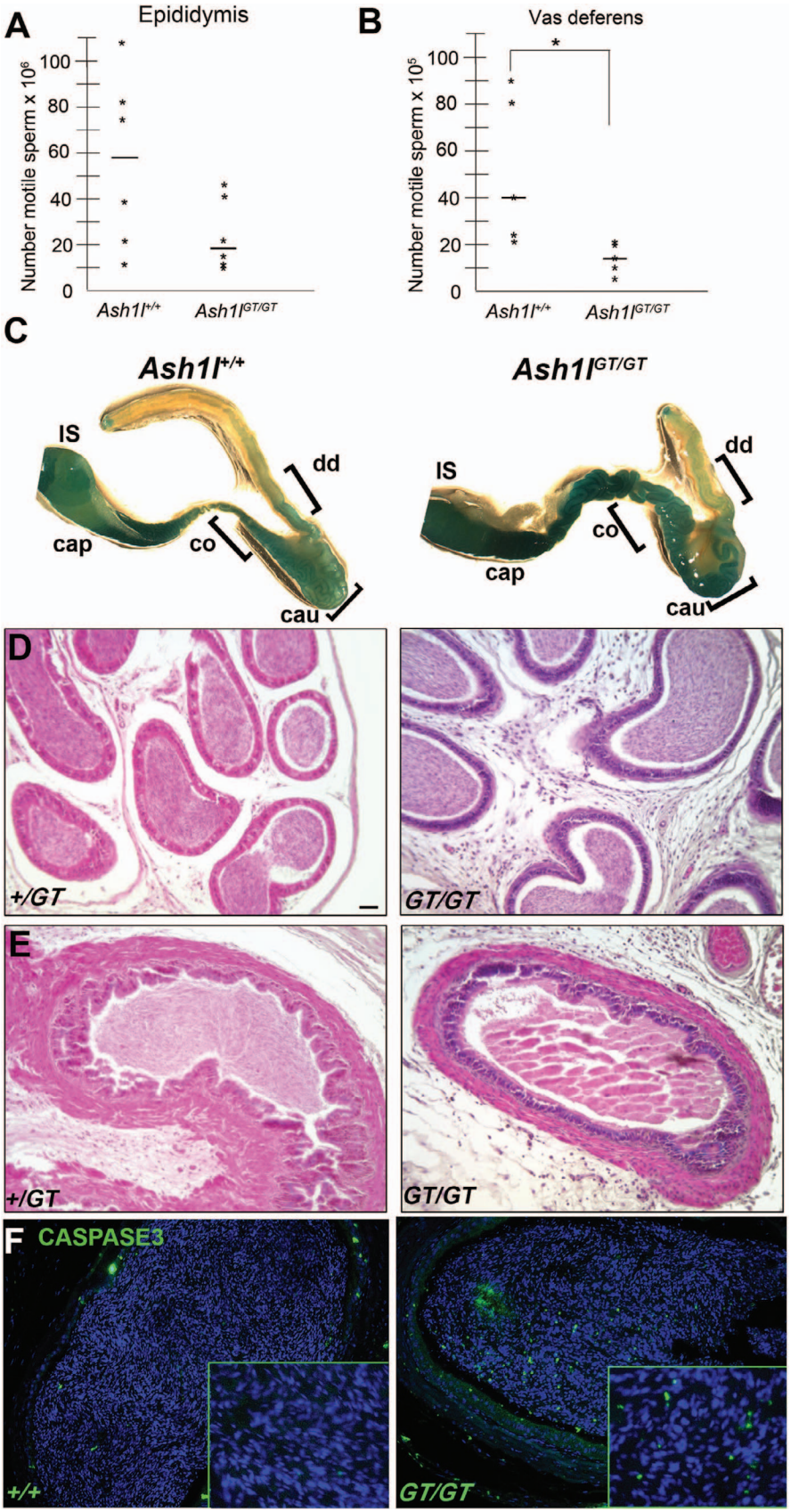

FIG. 3. *Ash1l*$^{GT/GT}$ males have reduced sperm in the vas deferens and abnormal epididymis morphology. Scatter plot graph of the number of motile sperm collected from the epididymis (**A**) and vas deferens (**B**) of individual *Ash1l*$^{+/+}$ and *Ash1l*$^{GT/GT}$ males. The bar represents the median of the group. **C**) X-Gal staining of whole mount epididymis from 3-mo-old *Ash1l*$^{+/+}$ and *Ash1l*$^{GT/GT}$ males. The regions of the epididymis are labeled: IS, initial segment; cap, caput; co, corpus; cau, cauda; and dd, ductus deferens. Hematoxylin and eosin staining on paraffin sections through the cauda (**D**) of the epididymis and the vas deferens (**E**) in 3-mo-old *Ash1l*$^{+/GT}$ and *Ash1l*$^{GT/GT}$ males. **F**) Cleaved CASPASE 3 immunostaining was used to detect apoptotic sperm in the lumen of the tubules in the ductus deferens in *Ash1l*$^{+/+}$ and *Ash1l*$^{GT/GT}$ males. Bar = 50 μm (**D**–**F**).

appeared wider, and the ductus deferens resembled the cauda [40].

Cross sections through the cauda and the vas deferens of *Ash1l*$^{+/GT}$ and *Ash1l*$^{GT/GT}$ males were stained with hematoxylin and eosin to analyze the morphology and detect the presence of sperm. The morphology was similar between *Ash1l*$^{+GT}$ and *Ash1l*$^{GT/GT}$ cauda (Fig. 3D), and sperm were identified in the lumen of tubules from both *Ash1l*$^{+/GT}$ and *Ash1l*$^{GT/GT}$ cauda. There were fewer sperm in the vas deferens of most *Ash1l*$^{GT/GT}$ males compared to *Ash1l*$^{+/GT}$ males (Fig. 3E). Sperm within the vas deferens were analyzed for cell death using an antibody to activated CASPASE 3. No apoptotic sperm were identified in *Ash1l*$^{+/+}$ vas deferens (n = 2), but apoptotic cells were identified in the vas deferens of all *Ash1l*$^{GT/GT}$ males (n = 6) (Fig. 3F). Thus, the *Ash1l*-deficient epididymis fails to nurture sperm and results in sperm death, which explains the reduced number of motile sperm in the mutant vas deferens.

Hox *Gene Expression Was Altered in* Ash1l$^{GT/GT}$ *Epididymis*

Defects in *Hox* gene expression are known to cause transformations of the epididymis that are similar to the structural abnormalities we observed in the *Ash1l* mutants, and some *Hox* genes exhibit region-specific expression in the reproductive tract [40]. ASH1L protein is present in the cells lining the tubules throughout the epididymis in *Ash1l*$^{+/+}$ (n = 2) mice, but it was either significantly reduced or absent from *Ash1l*$^{GT/GT}$ (n = 4) epididymal tubules (Fig. 4A). *Ash1l* transcripts were detectable in *Ash1l*$^{+/+}$ epididymis by real-time PCR and was reduced approximately 9-fold in *Ash1l*$^{GT/GT}$ epididymis (Fig. 4B). Developmentally important markers such as CYCLIND2 and CYCLIND1 were not affected by decreases in *Ash1l* (Fig. 4, C and D). Thus, the poor sperm maturation in the epididymis is linked to the reduced expression of *Ash1l* in the cells lining this tissue.

To determine whether the levels of *Ash1l* expression varied along the length of the epididymis, we quantified *Ash1l, Hoxa9, Hoxa10, Hoxa11, Hoxc4, Hoxc9, Hoxd10,* and *Hoxd13* in cDNA from systematically microdissected regions of 3-wk-old *Ash1l*$^{+/+}$ epididymis (Fig. 4E and Supplemental Fig. S4). CT levels from Taqman gene expression assays (Applied Biosystems) were compared to CT levels of *Gapdh* in each sample to evaluate the level of transcript in each segment of the epididymis and ductus deferens. *Ash1l, Hoxa9, Hoxc4,* and *Hoxd10* were expressed uniformly throughout the epididymis and ductus deferens. *Hoxa10, Hoxa11,* and *Hoxd13* were expressed at higher levels toward the end of the epididymis and into the ductus deferens. *Hoxc9* was expressed throughout the epididymis and ductus deferens with the highest levels in the corpus segment. These results are consistent with the previous reports of the expression of select *Hox* genes along the length of the epididymis and ductus deferens in adult and P1 mice [41, 42], and they suggest that *Ash1l* has the potential to affect *Hox* gene expression in all regions of the epididymis.

We hypothesized that *Ash1l* deficiency resulted in altered *Hox* gene expression. To determine if this could be the underlying mechanism, we used real-time quantitative RT-PCR to compare the expression of *Ash1l* and *Hox* genes in normal and mutant mice. We compared expression of *Ash1l, Hoxa9, Hoxa10, Hoxa11, Hoxc4, Hoxc9, Hoxd10,* and *Hoxd13* in the microdissected initial segment, caput, corpus, and cauda of the epididymis and the ductus deferens of *Ash1l*$^{+/+}$ (n = 6) and *Ash1l*$^{GT/GT}$ (n = 6) mice. As expected, *Ash1l* transcripts were significantly reduced in all segments of the epididymides and the ductus deferens of the mutants (data not shown). There was a significant decrease in expression of *Hoxd10* specifically in the initial segment, caput, and ductus deferens of the epididymis as well as significant decreases in *Hoxa11* in the initial segment of *Ash1l*$^{GT/GT}$ epididymis (Fig. 4F). Decreases in *Ash1l* and *Hoxa11* mRNA were confirmed by whole mount in situ hybridization in epididymis from 3-wk-old males (Fig. 4G). No differences in expression of *Hoxa9, Hoxa10, Hoxc4, Hoxc9,* and *Hoxd13* were observed between *Ash1l*$^{+/+}$ and *Ash1l*$^{GT/GT}$ in any segments of the epididymis (data not shown). The effect of reduced *Ash1l* on *Hoxd10* and *Hoxa11* expression within the epididymis and the loss of motile sperm within the ductus deferens suggested that *Ash1l* deficiency causes region-specific reduced *Hox* gene expression, which impairs sperm maturation within the epididymis and which results in infertility during natural mating.

DISCUSSION

Drosophila ash1 is an epigenetic regulator of HOX gene expression, and *ash1l* deficiency causes absent, small or homeotic transformation of many specific structures during development, including reproductive organs. The *ash1* gene is also important for adult organ function. Here we show that deficiency of the mammalian ortholog, *Ash1l*, also disrupts development and function of many organ systems and structures, and we present a detailed analysis of the effects on the male and female reproductive tracts. Most *Drosophila ash1* mutants are not viable, and *Ash1l*-deficient mice have reduced viability after the first week of life. There is a variable, small amount of normal *Ash1l* in the gene trap mutants due to exon skipping of the gene trap cassette; this is a hypomorphic allele. It is possible that the mutant mice would die earlier or with a higher penetrance if they had a complete loss of *Ash1l* transcripts. Hypomorphic alleles like this *Ash1l* gene trap often have the advantage of revealing the roles of genes later in development or in adults that would be precluded by early embryonic lethality. In addition, they can be valuable in predicting the range of clinical presentations that could occur in humans with reduced *ASH1L* activity.

Ash1l deficiency causes homeotic-like changes in both the axial skeleton and the epididymis. The thoracic vertebrae T8 exhibit an anterior transformation to T7, which is accompanied by the presence of an extra rib attached to the sternum on the right, left, or both sides. Mice with targeted disruptions in *Hox5, Hoxc8,* or *Hoxb9* all exhibit transformations in the axial skeleton that are similar to the T8 to T7 transformation characteristic of *Ash1l* mutants [43–45]. *Ash1l* mutants with a SET domain deletion exhibit vertebral abnormalities. There is a partially penetrant C2 to C1 vertebral transformation associated with posterior shifts in *Hoxb4* and *Hoxd4* expression boundaries [15]. We did not observe any change in C2–C1 vertebrae. The SET domain mutants also differ from the gene trap allele reported here in that they have normal fertility and viability up to 3–4 wk of age. The basis for the differences in axial skeleton development, fertility, and viability between these two mutant alleles may be attributable to the different modifications that were engineered. The *Ash1l* gene trap mice are hypomorphs with reduced levels of normal protein, while deletion of the SET domain would be expected to result in normal levels of a protein that lacks methyl transferase activity but retains domains involved in protein-protein and/or protein-DNA interactions. Differences in genetic background may also contribute [46]. Nevertheless, the phenotypes of both mouse *Ash1l* alleles emphasize the importance of ASH1L in

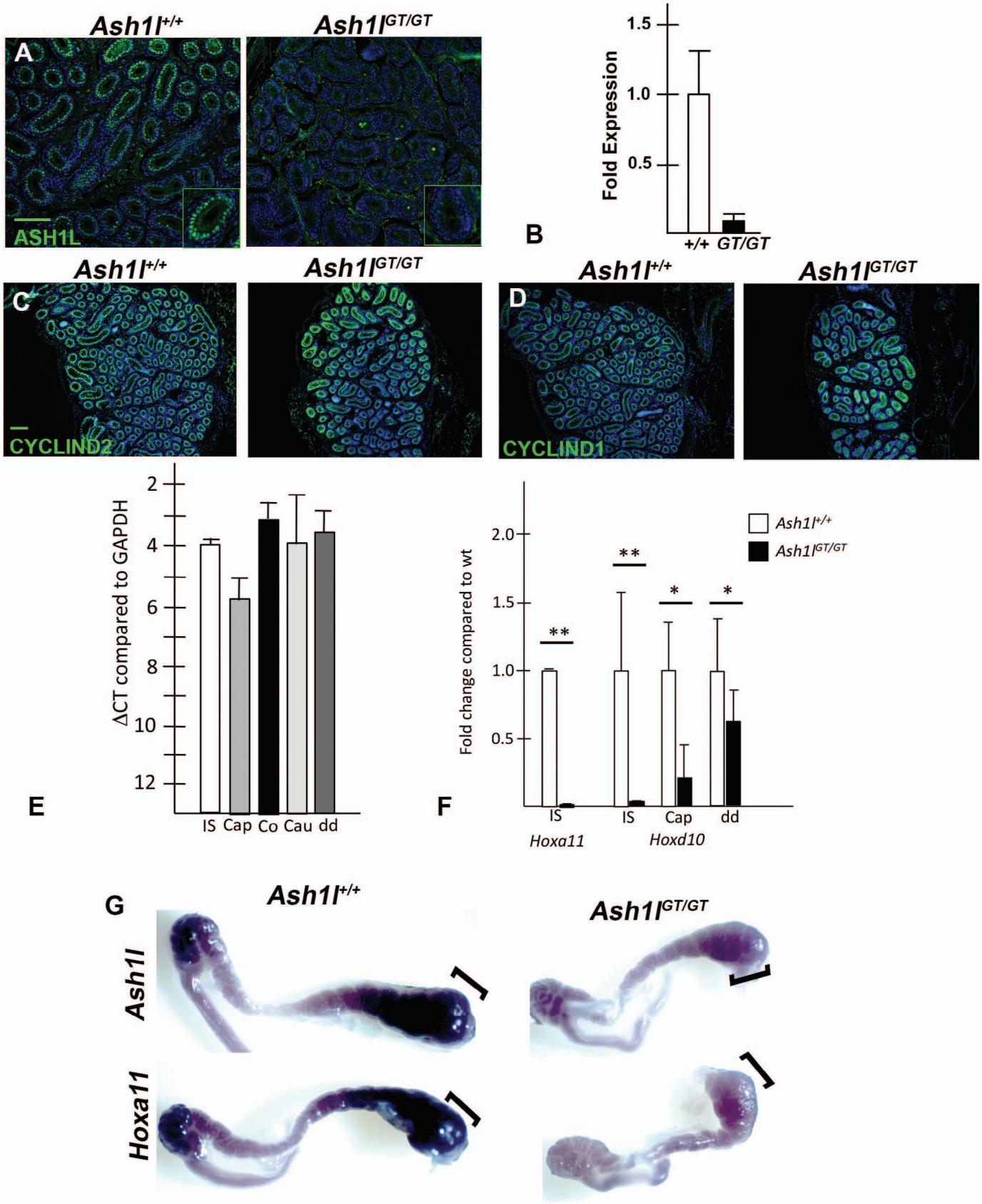

FIG. 4. Reduced levels of *Ash1l, Hoxd10,* and *Hoxa11* in the *Ash1l*$^{GT/GT}$ epididymis. **A**) ASH1L protein is expressed in the cells lining the tubules of the initial segment of the epididymis in *Ash1l*$^{+/+}$ mice but is substantially reduced in *Ash1l*$^{GT/GT}$ mice. The insets show magnified expression in a cross section of an individual tubule. Bar = 100 μm. **B**) *Ash1l* transcripts in the epididymis cDNA of 3-mo-old mice were measured by real-time PCR for three *Ash1l*$^{+/+}$ mice (white) and three *Ash1l*$^{GT/GT}$ mice (black) and presented as fold expression change compared to *Ash1l*$^{+/+}$. CYCLIND2 (**C**) and CYCLIND1 (**D**) immunohistochemistry on 3-wk-old *Ash1l*$^{+/+}$ and *Ash1l*$^{GT/GT}$ initial segments. Bar = 50 μm. **E**) Real-time PCR was used to detect *Ash1l* transcripts in

regulating expression of *Hox* genes that influence skeletal development.

The *Ash1l*$^{GT/GT}$ mutant females are completely infertile. Ovulation and estrus are normal, but uterine development is abnormal, and the mutant uteri are unable to support decidualization or implantation. *Ash1l* is normally expressed robustly in the uterine glands, which develop in response to progesterone beginning around P14 [47]. *Ash1l* deficiency nearly ablates the development of endometrial uterine glands, which are essential for fertility. These glands normally secrete leukemia inhibitory factor (*Lif*) and other factors that are required for embryo survival, implantation, and decidualization [48]. Other mouse mutants with missing or reduced uterine glands are infertile (reviewed in [39, 49]). Thus, the infertility of *Ash1l* mutant females can be explained by the failure to develop uterine glands prior to puberty.

Our data suggest a mechanism for *Ash1l* regulation of uterine development. Postnatally, *Ash1l* expression in the uterus likely activates expression of *Hoxa10* and other genes by histone methylation effects on chromatin. The expression of *Hoxa10* is substantially reduced in the stroma of the *Ash1l* mutants, and *Hoxa10* expression is affected by epigenetic control of DNA methylation [50]. *Hoxa10* exhibits dynamic expression during the estrus cycle and decidualization process, and the uteri of *Hoxa10* knockout mice are similar to those of female *Ash1l* mutants [35, 40]. *HOXA10* expression is altered in patients with endometriosis and women with nutritional deficits, two conditions that can cause infertility. Thus, our studies on the role of *Ash1l* in female infertility in mice could be relevant to human clinical problems.

Ash1l mutant males have a 90% reduction in fertility. *Ash1l* is necessary for prepubertal structural development of the epididymis and for epididymal function in supporting sperm maturation and motility. Between birth and puberty, the epididymis undergoes differentiation and segmentation, which is necessary to support the progressive maturation of spermatozoa as they move through the epididymis (reviewed in [51]). The fully mature and motile sperm are stored and protected in the coils of the cauda [37]. *Ash1l*$^{GT/GT}$ males exhibit abnormal coiling of the corpus and the ductus deferens consistent with a transformation from corpus to caput and ductus deferens to cauda. This structural abnormality is associated with reduced viability and motility of sperm as they travel through the epididymis.

Mechanistically, normal epididymal development likely involves *Ash1l* regulation of *Hoxa10, Hoxa11,* and other genes by histone methylation effects on chromatin. The final development of the epididymis is known to be regulated by *Hox* gene expression (reviewed in [51]), and prepubertal *Ash1l*$^{GT/GT}$ mutants have decreased expression of *Hoxa11* in the initial segment and *Hoxd10* in the initial segment, caput, and ductus deferens. *Hoxa11* is normally expressed at higher levels toward the caudal end of the epididymis, which is the site of transformation in *Ash1l* mutants. Both *Hoxa11* and the paralog of *Hoxd10,* that is, *Hoxa10,* are known to be critical for epididymis development and function [40, 52]. In conclusion, the role of *Ash1l* in male fertility is in the epididymis where it regulates *Hox* gene expression that is required for normal structural development, which is necessary to support sperm maturation and viability.

In *Drosophila, ash1* and *trx* work together to regulate gene expression through histone methylation. The mammalian orthologs of *trx* belong to the *Mll* family (reviewed in [53]), which also regulate expression of genes through histone methylation [54, 55]. If ASH1L interacts with MLL family members to regulate gene expression, we would expect to observe some similarities in the phenotypes associated with mutations in these genes and other regulators of chromatin structure. Indeed, many phenotypic characteristics of *Ash1l*-deficient mice are similar to the developmental defects in mouse knockout models of genes involved in chromatin remodeling. For example, four features of *Ash1l* mutants are recapitulated by targeted disruption of *Psip1,* also known as *Ledgf,* a chromatin-associated protein with specificity to H3K36 methylation. *Psip1* mutants exhibit postnatal lethality, reduced male fertility, chronic blepharitis, and decreased abdominal fat [56]. LEDGF interacts in a complex with MLL and Menin to regulate gene transcription in MLL-driven leukemia [57]. *Mll5*$^{-/-}$ mice exhibit reduced growth, postnatal lethality, male infertility, and chronic blepharitis, all features mimicked in *Ash1l* mutants [58, 59]. *Mll3*$^{-/-}$ mice have reduced body size and lack abdominal fat [6]. The similar features of these chromatin-associated proteins suggest they may interact with ASH1L to epigenetically regulate a set of genes that are important for similar processes.

Studies in *Drosophila* demonstrated the role of ASH1 in the regulation of homeotic genes during development and in adult organ function. We noted absent, small, and homeotic-like transformations in many structures and tissues in developing and prepubertal *Ash1l*-deficient mice, consistent with functional conservation in vertebrates and invertebrates. The role of homeobox genes is well-known in the development of mammalian reproductive organs and the axial skeleton, but mechanistic underpinnings are still emerging. Our report reveals a critical role for ASH1L in *Hox* gene expression for pubertal development and reproductive function in both males and females. Further analysis of the uterus and epididymis of ASH1L-deficient mice could uncover altered expression of numerous genes, including other transcription factors, signaling pathways, and/or the cell cycle regulators [50]. Despite the known global effects of epigenetic regulation on gene expression, *Ash1l* deficiency leads to very specific defects in organ development. Thus, human multiple congenital anomaly syndromes and/or infertility could be caused by defects in ASH1L or other chromatin-modifying proteins. The generation and characterization of this gene trap allele has revealed the essential role of ASH1L in epigenetic regulation of gene expression in reproductive organs.

ACKNOWLEDGMENT

We would like to thank the University of Michigan DNA Sequencing Core and the Transgenic Animal Model Core, including Thomas Saunders, Elizabeth Hughes, Galina Gavrilina, and the late Maggie Van Keuren, for their help with the generation of the gene trap mice and for their help with the fertility studies. We would like to thank Deneen Wellik for her help with skeletal analysis, Dr. Greg Gregory and Dr. Gerd Blobel for the

cDNA from systematically microdissected regions of the epididymis from *Ash1l*$^{+/+}$ mice. The bars represent the change in CT levels compared to *Gapdh* levels. IS, initial segment; Cap, caput; Co, corpus; Cau, cauda; and dd, ductus deferens. **F**) Real-time PCR was used to detect *Hoxd10* and *Hoxa11* transcripts in cDNA from dissected regions of the epididymis in 3-wk-old *Ash1l*$^{+/+}$ males (n = 6, white) and *Ash1l*$^{GT/GT}$ males (n = 6, black). The bars represent the fold change relative to *Ash1l*$^{+/+}$. White bars represent *Ash1l*$^{+/+}$ and black bars represent *Ash1l*$^{GT/GT}$. **G**) Whole mount in situ hybridization of *Ash1l* and *Hoxa11* in 3-wk-old epididymis in *Ash1l*$^{+/+}$ and *Ash1l*$^{GT/GT}$. Bracketed region highlights the initial segment.

ASH1L 296 antibody, and Sundeep Kalantry, Barry Hinton, Gerd Blobel, and Greg Gregory for their input on the project.

REFERENCES

1. Butler JS, Koutelou E, Schibler AC, Dent SY. Histone-modifying enzymes: regulators of developmental decisions and drivers of human disease. Epigenomics 2012; 4:163–177.
2. Greer EL, Shi Y. Histone methylation: a dynamic mark in health, disease and inheritance. Nat Rev Genet 2012; 13:343–357.
3. Albert M, Helin K. Histone methyltransferases in cancer. Semin Cell Dev Biol 2010; 21:209–220.
4. McMahon KA, Hiew SY, Hadjur S, Veiga-Fernandes H, Menzel U, Price AJ, Kioussis D, Williams O, Brady HJ. Mll has a critical role in fetal and adult hematopoietic stem cell self-renewal. Cell Stem Cell 2007; 1: 338–345.
5. Glaser S, Schaft J, Lubitz S, Vintersten K, van der Hoeven F, Tufteland KR, Aasland R, Anastassiadis K, Ang SL, Stewart AF. Multiple epigenetic maintenance factors implicated by the loss of Mll2 in mouse development. Development 2006; 133:1423–1432.
6. Lee J, Saha PK, Yang QH, Lee S, Park JY, Suh Y, Lee SK, Chan L, Roeder RG, Lee JW. Targeted inactivation of MLL3 histone H3-Lys-4 methyltransferase activity in the mouse reveals vital roles for MLL3 in adipogenesis. Proc Natl Acad Sci U S A 2008; 105:19229–19234.
7. Klymenko T, Muller J. The histone methyltransferases Trithorax and Ash1 prevent transcriptional silencing by Polycomb group proteins. EMBO Rep 2004; 5:373–377.
8. Papp B, Muller J. Histone trimethylation and the maintenance of transcriptional ON and OFF states by trxG and PcG proteins. Genes Dev 2006; 20:2041–2054.
9. Paro R. Mechanisms of heritable gene repression during development of Drosophila. Curr Opin Cell Biol 1993; 5:999–1005.
10. Petruk S, Smith ST, Sedkov Y, Mazo A. Association of trxG and PcG proteins with the bxd maintenance element depends on transcriptional activity. Development 2008; 135:2383–2390.
11. Byrd KN, Shearn A. ASH1, a Drosophila trithorax group protein, is required for methylation of lysine 4 residues on histone H3. Proc Natl Acad Sci U S A 2003; 100:11535–11540.
12. Dorighi KM, Tamkun JW. The trithorax group proteins Kismet and ASH1 promote H3K36 dimethylation to counteract Polycomb group repression in Drosophila. Development 2013; 140:4182–4192.
13. Xia M, Liu J, Wu X, Liu S, Li G, Han C, Song L, Li Z, Wang Q, Wang J, Xu T, Cao X. Histone methyltransferase Ash1l suppresses interleukin-6 production and inflammatory autoimmune diseases by inducing the ubiquitin-editing enzyme A20. Immunity 2013; 39:470–481.
14. Gregory GD, Vakoc CR, Rozovskaia T, Zheng X, Patel S, Nakamura T, Canaani E, Blobel GA. Mammalian ASH1L is a histone methyltransferase that occupies the transcribed region of active genes. Mol Cell Biol 2007; 27:8466–8479.
15. Miyazaki H, Higashimoto K, Yada Y, Endo TA, Sharif J, Komori T, Matsuda M, Koseki Y, Nakayama M, Soejima H, Handa H, Koseki H, et al. Ash1l methylates Lys36 of histone H3 independently of transcriptional elongation to counteract polycomb silencing. PLoS Genet 2013; 9: e1003897.
16. Tripoulas NA, Hersperger E, La Jeunesse D, Shearn A. Molecular genetic analysis of the Drosophila melanogaster gene absent, small or homeotic discs1 (ash1). Genetics 1994; 137:1027–1038.
17. Shearn A. The ash-1, ash-2 and trithorax genes of Drosophila melanogaster are functionally related. Genetics 1989; 121:517–525.
18. Ali M, Hom RA, Blakeslee W, Ikenouye L, Kutateladze TG. Diverse functions of PHD fingers of the MLL/KMT2 subfamily. Biochim Biophys Acta 2014; 1843:366–371.
19. Rozovskaia T, Tillib S, Smith S, Sedkov Y, Rozenblatt-Rosen O, Petruk S, Yano T, Nakamura T, Ben-Simchon L, Gildea J, Croce CM, Shearn A, et al. Trithorax and ASH1 interact directly and associate with the trithorax group-responsive bxd region of the Ultrabithorax promoter. Mol Cell Biol 1999; 19:6441–6447.
20. Nakamura T, Blechman J, Tada S, Rozovskaia T, Itoyama T, Bullrich F, Mazo A, Croce CM, Geiger B, Canaani E. huASH1 protein, a putative transcription factor encoded by a human homologue of the Drosophila ash1 gene, localizes to both nuclei and cell-cell tight junctions.Proc Natl Acad Sci U S A 2000; 97:7284–7289.
21. Skarnes WC, Moss JE, Hurtley SM, Beddington RS. Capturing genes encoding membrane and secreted proteins important for mouse development. Proc Natl Acad Sci U S A 1995; 92:6592–6596.
22. Hogan B, Beddington R, Costantini F, Recovery, Lacy E. Culture, and transfer of embryos. In: Manipulating the Mouse Embryo, 2nd ed. Plainview, NY: Cold Spring Harbor Laboratory Press; 1994:128–132.
23. Hogan B, Beddington R, Costantini F, Lacy E. Summary of mouse development. In: Manipulating the Mouse Embryo, 2nd ed. Plainview, NY: Cold Spring Harbor Laboratory Press; 1994:20–113.
24. Mortensen AH, Schade V, Lamonerie T, Camper SA. Deletion of OTX2 in neural ectoderm delays anterior pituitary development. Hum Mol Genet 2015; 24:939–953.
25. Suh H, Gage PJ, Drouin J, Camper SA. Pitx2 is required at multiple stages of pituitary organogenesis: pituitary primordium formation and cell specification. Development 2002; 129:329–337.
26. Byers SL, Payson SJ, Taft RA. Performance of ten inbred mouse strains following assisted reproductive technologies (ARTs). Theriogenology 2006; 65:1716–1726.
27. Suzuki H, Yorozu K, Watanabe T, Nakura M, Adachi J. Rederivation of mice by means of in vitro fertilization and embryo transfer. Exp Anim 1996; 45:33–38.
28. Whittingham DG. Fertilization of mouse eggs in vitro. Nature 1968; 220: 592–593.
29. Jelinsky SA, Turner TT, Bang HJ, Finger JN, Solarz MK, Wilson E, Brown EL, Kopf GS, Johnston DS. The rat epididymal transcriptome: comparison of segmental gene expression in the rat and mouse epididymides. Biol Reprod 2007; 76:561–570.
30. Brinkmeier ML, Davis SW, Carninci P, MacDonald JW, Kawai J, Ghosh D, Hayashizaki Y, Lyons RH, Camper SA. Discovery of transcriptional regulators and signaling pathways in the developing pituitary gland by bioinformatic and genomic approaches. Genomics 2009; 93:449–460.
31. Jones M, Chase J, Brinkmeier M, Xu J, Weinberg DN, Schira J, Friedman A, Malek S, Grembecka J, Cierpicki T, Dou Y, Camper SA, et al. Ash1l controls quiescence and self-renewal potential in hematopoietic stem cells. J Clin Invest 2015; 125:2007–2020.
32. Zieske JD. Corneal development associated with eyelid opening. Int J Dev Biol 2004; 48:903–911.
33. Kenchegowda D, Swamynathan S, Gupta D, Wan H, Whitsett J, Swamynathan SK. Conditional disruption of mouse Klf5 results in defective eyelids with malformed meibomian glands, abnormal cornea and loss of conjunctival goblet cells. Dev Biol 2011; 356:5–18.
34. Jeong JW, Kwak I, Lee KY, Kim TH, Large MJ, Stewart CL, Kaestner KH, Lydon JP, DeMayo FJ. *Foxa2* is essential for mouse endometrial gland development and fertility. Biol Reprod 2010; 83:396–403.
35. Lim H, Ma L, Ma WG, Maas RL, Dey SK. Hoxa-10 regulates uterine stromal cell responsiveness to progesterone during implantation and decidualization in the mouse. Mol Endocrinol 1999; 13:1005–1017.
36. Ma L, Benson GV, Lim H, Dey SK, Maas RL. Abdominal B (AbdB) Hoxa genes: regulation in adult uterus by estrogen and progesterone and repression in Mullerian duct by the synthetic estrogen diethylstilbestrol (DES). Dev Biol 1998; 197:141–154.
37. Buffone MG, Ijiri TW, Cao W, Merdiushev T, Aghajanian HK, Gerton GL. Heads or tails? Structural events and molecular mechanisms that promote mammalian sperm acrosomal exocytosis and motility. Mol Reprod Dev 2012; 79:4–18.
38. Gatti JL, Castella S, Dacheux F, Ecroyd H, Metayer S, Thimon V, Dacheux JL. Post-testicular sperm environment and fertility. Anim Reprod Sci 2004; 82-83:321–339.
39. Yoshinaga K. A sequence of events in the uterus prior to implantation in the mouse. J Assist Reprod Genet 2013; 30:1017–1022.
40. Benson GV, Lim H, Paria BC, Satokata I, Dey SK, Maas RL. Mechanisms of reduced fertility in Hoxa-10 mutant mice: uterine homeosis and loss of maternal Hoxa-10 expression. Development 1996; 122:2687–2696.
41. Snyder EM, Small CL, Bomgardner D, Xu B, Evanoff R, Griswold MD, Hinton BT. Gene expression in the efferent ducts, epididymis, and vas deferens during embryonic development of the mouse. Dev Dyn 2010; 239:2479–2491.
42. Bomgardner D, Hinton BT, Turner TT. 5′ hox genes and meis 1, a hox-DNA binding cofactor, are expressed in the adult mouse epididymis. Biol Reprod 2003; 68:644–650.
43. McIntyre DC, Rakshit S, Yallowitz AR, Loken L, Jeannotte L, Capecchi MR, Wellik DM. Hox patterning of the vertebrate rib cage. Development 2007; 134:2981–2989.
44. Juan AH, Lei H, Bhargava P, Lebrun M, Ruddle FH. Multiple roles of hoxc8 in skeletal development. Ann N Y Acad Sci 2006; 1068:87–94.
45. Chen F, Capecchi MR. Targeted mutations in hoxa-9 and hoxb-9 reveal synergistic interactions. Dev Biol 1997; 181:186–196.
46. Doetschman T. Influence of genetic background on genetically engineered mouse phenotypes. Methods Mol Biol 2009; 530:423–433.
47. Fernandez-Valdivia R, Mukherjee A, Mulac-Jericevic B, Conneely OM, De Mayo FJ, Amato P, Lydon JP. Revealing progesterone's role in uterine

and mammary gland biology: insights from the mouse. Semin Reprod Med 2005; 23:22–37.
48. Filant J, Spencer TE. Endometrial glands are essential for blastocyst implantation and decidualization in the mouse uterus. Biol Reprod 2013; 88:93.
49. Cooke PS, Spencer TE, Bartol FF, Hayashi K. Uterine glands: development, function and experimental model systems. Mol Hum Reprod 2013; 19:547–558.
50. Das SK. Regional development of uterine decidualization: molecular signaling by Hoxa-10. Mol Reprod Dev 2010; 77:387–396.
51. Kirchhoff C. Gene expression in the epididymis. Int Rev Cytol 1999; 188: 133–202.
52. Hsieh-Li HM, Witte DP, Weinstein M, Branford W, Li H, Small K, Potter SS. Hoxa 11 structure, extensive antisense transcription, and function in male and female fertility. Development 1995; 121:1373–1385.
53. Gould A. Functions of mammalian Polycomb group and trithorax group related genes. Curr Opin Genet Dev 1997; 7:488–494.
54. Ansari KI, Mandal SS. Mixed lineage leukemia: roles in gene expression, hormone signaling and mRNA processing. FEBS J 2010; 277:1790–1804.
55. Dou Y, Milne TA, Ruthenburg AJ, Lee S, Lee JW, Verdine GL, Allis CD, Roeder RG. Regulation of MLL1 H3K4 methyltransferase activity by its core components. Nat Struct Mol Biol 2006; 13:713–719.
56. Sutherland HG, Newton K, Brownstein DG, Holmes MC, Kress C, Semple CA, Bickmore WA. Disruption of Ledgf/Psip1 results in perinatal mortality and homeotic skeletal transformations. Mol Cell Biol 2006; 26: 7201–7210.
57. Yokoyama A, Cleary ML. Menin critically links MLL proteins with LEDGF on cancer-associated target genes. Cancer Cell 2008; 14:36–46.
58. Heuser M, Yap DB, Leung M, de Algara TR, Tafech A, McKinney S, Dixon J, Thresher R, Colledge B, Carlton M, Humphries RK, Aparicio SA. Loss of MLL5 results in pleiotropic hematopoietic defects, reduced neutrophil immune function, and extreme sensitivity to DNA demethylation. Blood 2009; 113:1432–1443.
59. Madan V, Madan B, Brykczynska U, Zilbermann F, Hogeveen K, Dohner K, Dohner H, Weber O, Blum C, Rodewald HR, Sassone-Corsi P, Peters AH, et al. Impaired function of primitive hematopoietic cells in mice lacking the Mixed-Lineage-Leukemia homolog MLL5. Blood 2009; 113: 1444–1454.